PHYSICAL REVIEW ACCELERATORS AND BEAMS **25,** 060101 (2022)

Editors' Suggestion

Commissioning of a high power linac at GANIL: Beam power ramp-up

A. K. Orduz,* M. Di Giacomo, R. Ferdinand, B. Jacquot, O. Kamalou,
J-M. Lagniel, G. Normand, and A. Savalle
GANIL, CEA/DRF-CNRS/IN2P3, BP 55027, F-14076 Caen Cedex 5, France

D. Uriot
IRFU, CEA, Université Paris-Saclay, F-91191 Gif-sur-Yvette, France

(Received 29 March 2022; accepted 23 May 2022; published 14 June 2022)

SPIRAL2 is a high power linear accelerator part of the GANIL laboratory. This superconducting (SC) linac can accelerate cw light ions to heavy ions at energies up to 40 MeV/nucleon and 14.5 MeV/nucleon, respectively. In July 2019, the authorization to fully operate the SPIRAL2 SC linac permitted to start the commissioning of the medium energy beam transport line and SC linac. The main milestone of the commissioning in 2020 was to validate the transport and linac design by increasing the duty cycle up to 10% with a proton beam. This paper presents the strategy used by the commissioning team to increase the beam power, as well as the results obtained using different diagnostics. The extrapolation from obtained measurements to 100% duty cycle was also performed; the results are presented.

DOI: 10.1103/PhysRevAccelBeams.25.060101

I. INTRODUCTION

GANIL (Grand Accélérateur National d'Ions Lourds) produces stable and radioactive beams since 1983 using an accelerator complex that currently comprises five cyclotrons, numerous versatile detection facilities, and its major upgrade, SPIRAL2 (Système de Production d'Ions RAdioactifs en Ligne de 2e generation). SPIRAL2 will provide higher levels of production and precision than existing ones, allowing studying unknown properties of exotic nuclei at the limits of the periodic table. It will open up in GANIL new areas of research with beams of energetic neutrons, to deepen and broaden the study of the fission process [1]. The flux of neutrons at Neutrons For Science (NFS) will be up to 2 orders of magnitude higher than those of other existing time-of-flight facilities for a part spectrum in the 1–40 MeV range. These energies are well suited for studies on the transmutation of nuclear waste in ADS or in the new generation fast reactors and the effect of neutrons on materials and biological systems, among others. The intensity and variety of beams (charged particles and neutrons) delivered by the cyclotrons and the LINAC make it the only facility in the world today providing all these beams at the same center, thus making it a unique multidisciplinary facility [2].

The SPIRAL2 SC linac layout is shown in Fig. 1. It is composed of two injectors, one for light ions (H^+, $^2H^+$) and one for heavy ions ($A/Q \leq 3$), an Radio Frequency Quadrupole (RFQ) to accelerate beams up to 0.73 MeV/nucleon, a medium energy beam transport (MEBT) line, an SC linac with 26 cavities, and high energy beam transport (HEBT) lines [3]. The beams are driven up to SAFARI (optimized beam stop device for high intensity beams) [4] or to the experimental halls: NFS for neutron beam production [5] and S3 (Super Separator Spectrometer) for in-flight radioactive ion beam production [6,7]. The parameters of the different SPIRAL2 SC linac beams are listed in Table I.

The SPIRAL2 SC linac [8,9] includes 12 A-type cryomodules, each comprising one low-β cavity ($\beta = 0.07$, developed by Commissariat à l'énergie atomique et aux énergies alternatives/Institut de recherche sur les lois fondamentales de l'Univers (CEA)/IRFU [10]) and 7 B-type cryomodules, each comprising two high-β cavities ($\beta = 0.12$, developed by IJCLab [11]).

The commissioning of the Low Energy Beam Transport lines LEBT1 and LEBT2, RFQ, and diagnostics started in 2014 in parallel with the installation of the SC linac. During the first stages of the commissioning, beams from H^+ to $^{18}O^{6+}$ were studied with the diagnostic plate [12]. The MEBT line commissioning started after the full operation authorization by the French nuclear safety authority in July 2019 and the SC linac beam tuning started after the internal authorization was obtained on October 28th of the same year.

The MEBT line and the single bunch selector (SBS) were commissioned with H^+ and $^4He^{2+}$ beams [13,14].

---

*Corresponding author.
angie.orduz@ganil.fr

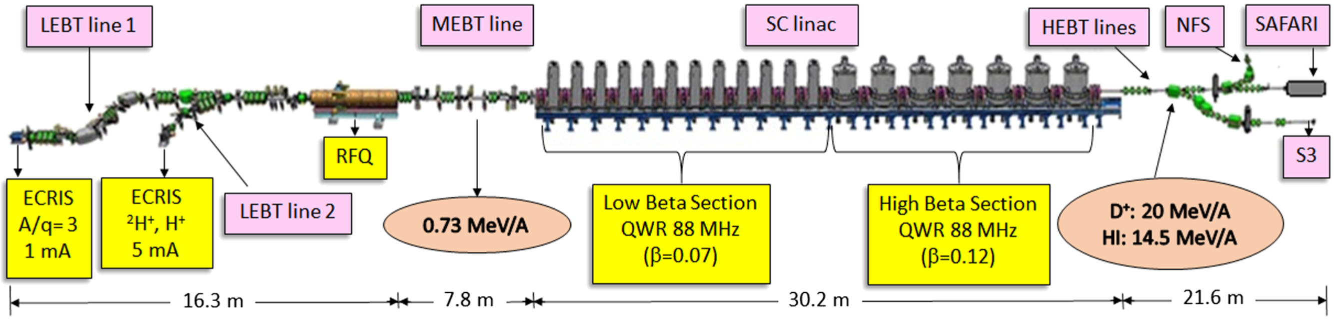

FIG. 1. SPIRAL2 SC linac layout.

The SBS is a system that reduces by a factor ranging from 100 to 50000 the bunch repetition rate. It is based on a static magnetic field deviating the beam on a 7.3 kW beam dump and travelling wave pulsed electric field selecting one bunch to stay on the beam axis. This SBS is mainly required for the time-of-flight measurement but is also used to reduce the power of the beam pulsed by the LEBT chopper on the HEBT profilers. The tuning of the SC linac and NFS HEBT line was also successfully performed with a 5 mA proton beam and the first experiment in the NFS experimental room could start. In 2020, the beam power was ramped-up to 10% of the maximum power (165 kW), transporting the proton beam to the SAFARI beam dump.

This paper focuses on the strategy and results of the beam power ramp-up. The first part describes the power increase strategy, the matching between the MEBT line and the SC linac, and the low level rf (LLRF) improvement. Finally, the extrapolation to 100% duty cycle is presented.

II. MAIN DIAGNOSTICS USED TO ANALYZE BEAM LOSSES

In order to analyze and limit beam losses in the SC linac and HEBT line, the diagnostics presented in Fig. 2 are used to measure: (i) the transmission with the ac and dc current transformers (ACCT and DCCT) [15], (ii) the loss variations by the beam loss monitor (BLM), (iii) the pressure variations with the vacuum gauges, (iv) the beam transport in the SC linac with the beam position and ellipticity measured by the beam position monitor (BPM) [16], and (v) the temperature increase by the SAFARI thermocouples [4]. The diagnostics along the low and high β sections of the SC linac are located in the middle of the RT quadrupoles between the cryomodules (warm sections).

TABLE I. Beam parameters at SPIRAL2 SC linac.

Particles	H^+	$^2H^+$	Ions
A/Q	1	2	3
Max I (mA)	5	5	1
Max E (MeV/nucleon)	33	20	14.5
Beam power (kW)	165	200	45

A. ACCT/DCCT current transformers

Three ACCT/DCCT are installed at the entrance and exit of the SC linac and at the SAFARI entrance. The main parameters of the transformers are summarized in Table II [15].

Even in “cw” mode, the choice was to maintain a pulsed mode with the LEBT chopper switching off the beam for 200 μs at each repetition period (1 Hz typically). This allows measuring the offset of the ACCT, whose accuracy is 6 μA at 1 Hz and 1 μA at 100 Hz, and allows a safer control of the beam power. The above mentioned absence of beam for 200 μs has no impact on the measurements, but all the transient times may lead to increased beam losses along the linac so have to be considered.

B. Beam loss monitors

The BLM system consists of 27 fixed scintillator detectors to monitor the beam losses along the SC linac and HEBT lines. According to the legislation for the safety of a nuclear facility, the BLMs are classified as equipment for protection against exposure to radiation. The associated safety requirements are (i) limit neutron radiation in accessible areas during operation and (ii) limit gamma radiation induced by the activation of the linac and transport lines.

As shown in Fig. 2, the BLMs are located along the SC linac warm sections and HEBT lines. Simulations were performed to evaluate the neutron flux at each BLM position, quantifying the thresholds corresponding to a 1 W/m beam loss for proton or deuteron beams. To calculate the light generated in the scintillator of each of the 27 BLMs, the Monte Carlo N-Particle (MCNP6) radiation-transport code was used [17]. The BLMs were also calibrated with two gamma and one neutron source (^{137}Cs, ^{60}Co, and Am-Be sources). It should be pointed out that the simulations take into account the thermal neutrons which also arise from the main beam dump. Below 10 MeV for protons and 7 MeV for deuterons, the neutron production is negligible, so loss measurements were not considered. Therefore, below 10 MeV, it is difficult from the measurements of the BLMs to separate the neutron production resulting from

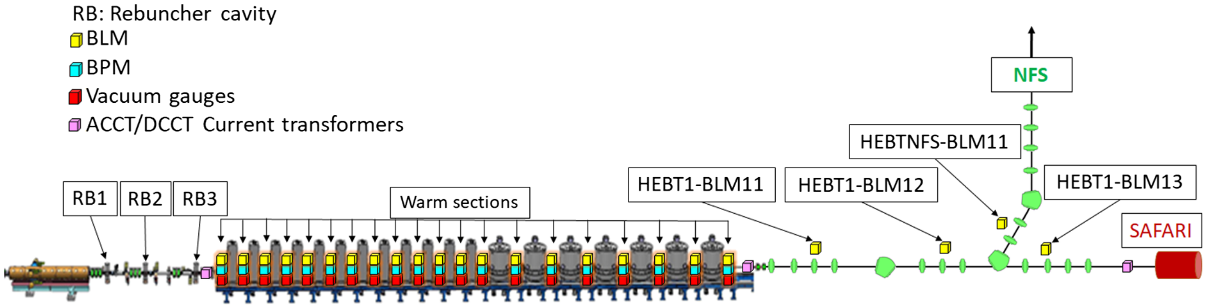

FIG. 2. Beam diagnostics in the SPIRAL2 SC linac used for the beam power ramp-up.

beam loss and from x ray arising from the cavities. In 2021, the BLM system was improved to ensure that the measurements take into account the neutrons produced by reactions, excluding cavity x rays and thermal neutrons. This was done from a calibration carried out with a ^{60}Co source adjusting the discriminator threshold in each detector to 1 MeV.

C. Pressure variations along the SC linac

Ion-induced desorption causes outgassing occurring when an ion beam interacts with the chambers [18]. Based on this process, beam losses can be related to the pressure variation for a given beam. However, although there are studies that describe these effects, calibrations are lacking to establish a relationship with the losses in W, as it is complicated because it depends on the nature of the ion, its energy, and the irradiated material [19]. Currently, several laboratories (CERN, GSI, GANIL, …) are carrying out studies to evaluate desorption yields, where the amount of desorbed gas molecules is derived from the pressure inside the vacuum vessel. Nevertheless, pressure variation has proved to be a valuable tool to control and decrease the amount of losses in the SPIRAL2 SC linac in addition to the BLMs or when BLMs cannot be used. In particular, in the low β section, i.e., when the energy is not high enough to produce neutrons, the vacuum response to beam loss is very sensitive.

The pressure is not measured in the cavity itself, since the associate cryogenic pumping is very efficient, but in the warm section in between the cryomodules, where the beam is transversally larger. The measurements taken into account are the pressure differences with and without beam.

TABLE II. Main uncertainties in the measurement of the average intensities.

Sources of uncertainty	ACCT	DCCT
Gain and linearity	0.6%	1%
Sensor temperature	…	8 μA[a]
Electronic temperature	…	23 μA[b]
Noise[c]	5.2 μA	4 μA

[a] DCCT range 20 mA, thermal regulation at 40°C ± 0.3°C.
[b] Ambient temperature range: 18–31°C.
[c] Noise measured over 1 s of acquisition without beam.

III. BEAM POWER RAMP-UP STRATEGY

The SPIRAL2 SC linac beam commissioning was organized in five phases as shown in Fig. 3. In the first phase, the beam is transported along all cavities of the SC linac tuned in rebuncher mode. This allowed a repetitive tuning of the cavities at a low beam power with no risks. In the second phase, the beam is accelerated to the maximum energy with an intensity low enough to limit the final beam power below 10 W. During the third phase, the beam intensity is ramped-up to a maximum value in order to correct the space charge and emittance increase effects. Finally, in the last phase, the maximum beam power is raised by increasing the duty cycle (pulse length and repetition rate).

From October 28 to November 15, 2019, started the first tuning phase at the RFQ energy (rebuncher mode) with a 1 W proton beam. Two weeks later phase 2 was achieved at 33 MeV (nominal energy) with a 6.4 W pencil beam of 250 μA and 0.1% duty cycle. It allowed to do the first NFS test experiment on December 5, the proton beam was sent

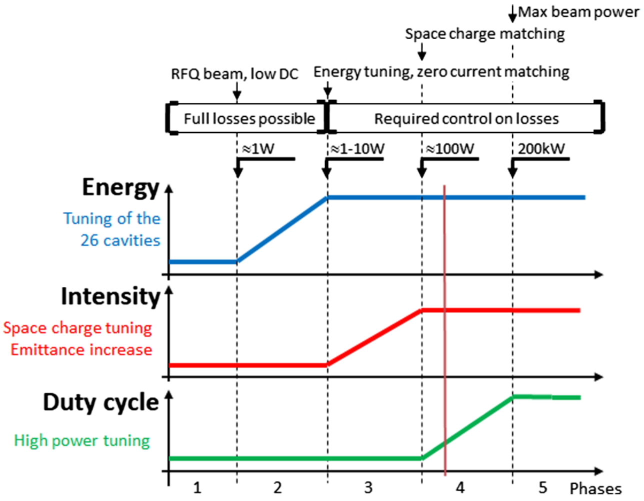

FIG. 3. Phases of the beam power ramp-up for the SPIRAL2 SC linac commissioning.

TABLE III. Beam parameters for the beam power ramp-up.

Beam power	2 kW	10 kW	16 kW
Energy (MeV)	31.90 ± 0.05	31.90 ± 0.05	31.90 ± 0.05
Intensity (mA)	4.35 ± 0.22	4.10 ± 0.21	4.00 ± 0.20
Pulse repetition (Hz)	1	10	10
Pulse length (ms)	14.5	7.7	12.6
Duty cycle (%)	1.5	7.7	12.6

to two beryllium and lithium targets to produce the first quasi-mono-energetic neutrons [1]. Phase 3 was reached on October 10, 2020, with a 4.8 mA proton beam, including all the space-charge difficulties and a much bigger emittance. The beam power ramp-up started afterward.

Three major power increase stages were performed during the commissioning in 2020, first to 2 kW, then to 10 kW, and finally to 16 kW. As shown in Table III, 16 kW was achieved with 12.6 ms pulse length every 100 ms (duty cycle = 12.6%, highest peak intensity and largest emittance). This pulse length is much larger than the time required to damage the chamber (35 μs for concentrated loss at nominal power) or for the rf systems to stabilize after transients (few ms). Then, increasing this length should not affect anymore the rf stability but only the amount of beam loss. The beam energy at the SC linac end was 31.9 MeV and not 33 MeV (nominal energy for H^+) because the last cavity of the SC linac was not used, due to one amplifier was out of order. Furthermore, the intensity in each of the stages was limited due to a technical limitation related to insufficient feedback of the rf amplifier power supply.

The main objective was to accelerate and transport a proton beam in order to validate the linac tuning, the diagnostics, and to do the radioprotection measurements. As presented in Fig. 4, 16 kW was achieved on October 18. The duration at 16 kW was limited only by the safety rules of GANIL to avoid the beam dump activation which leads to a maximum particle fluence of 5.62×10^{18} per 24 hours.

Between each stage of the beam power ramp-up, various systems were optimized, as described later in this document. The beam longitudinal and transverse matching between the MEBT line and the SC linac was done to reduce the beam losses at 2 kW beam power. The most significant contribution to loss reduction was the improvement of the LLRF system by increasing the gain of the feedback loops and mainly adding feedforward. Several simulations were performed with TRACEWIN [20] in order to compare and progress through each power ramp-up stage. Subsequently, the remaining losses were minimized using the transmission monitoring (ACCT and DCCT), BLMs, BPMs, and pressure variations in warm sections.

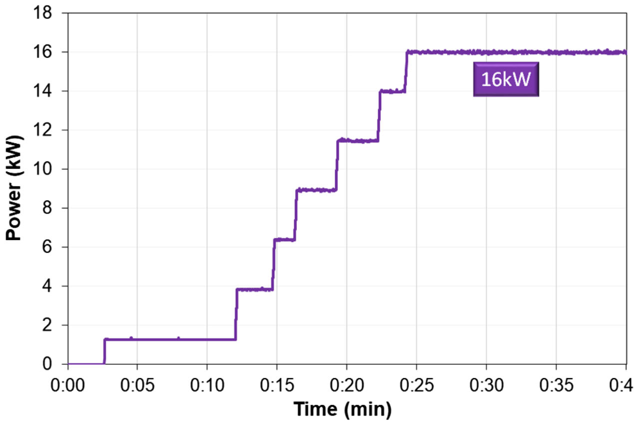

FIG. 4. Beam power ramp-up to 16 kW.

IV. MEBT-LINAC MATCHING

Various beam dynamics configurations (different beam and energies) were simulated for the SC linac, whose design is optimized for $^2H^+$ at 40 MeV. The 5 mA H^+ beam transport with 700 000 particles is presented in Fig. 5. The beam transverse rms emittance measured by an Allison emittance meter in the MEBT line for a 4 mA proton beam was $0.2\,\pi$ mm mrad.

A. Transverse plane matching

The MEBT line was tuned using the SC linac diagnostics. The last two quadrupoles of the line were adjusted while looking at the beam position and ellipticity and minimizing losses. The ellipticity trend was in agreement with the simulations as shown in Fig. 6, even if there is some beam mismatch still present at the SC linac entrance. Room for improvement still exists.

The reference value of the beam transverse phase advance is 80° in the low β section (at 0 mA) and decreases to 60° at 5 mA. The phase advance was measured at 16 kW using a small oscillation at the SC linac entrance. Figure 7

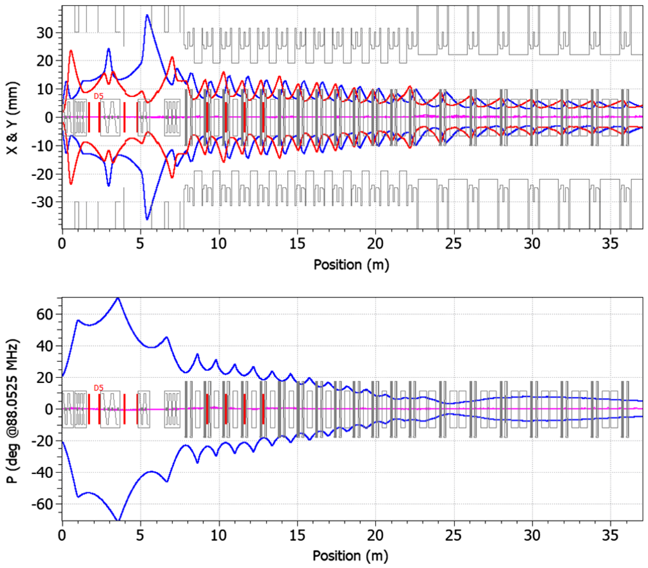

FIG. 5. Three rms envelopes from multiparticle simulation for the reference proton beam.

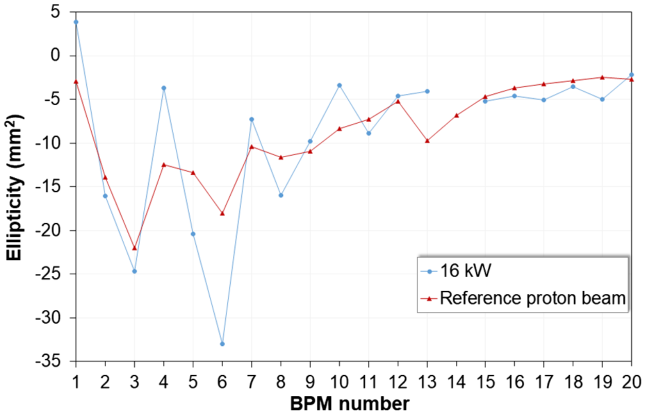

FIG. 6. Ellipticity for the 16 kW beam power (blue) and for the reference proton beam (red).

illustrates the agreement with the design in the vertical plane.

Losses were decreased especially in the low β section of the SC linac. The reduction was not highlighted by a diminution of the BLMs count rate but was confirmed by a reduction of the pressure variation up to 62% (warm section #9), as shown in Fig. 8. This clearly indicates that the associated losses were mostly located in the low β section and in the transition between low and high β sections where the acceptance is reduced.

The absolute error was estimated in a specific study performed to observe the pressure variation by intentionally losing 1 W of the beam in the SC linac. The pressure variation error bars include an absolute measurement error of ±30% and an instrument reproducibility of 5%. The error bar of warm section #8 is related to the relatively high absolute pressure.

B. Longitudinal plane matching

The bunch length measurements have been done with bunch extension monitors (BEM) located in the first five SC linac warm sections. During earlier commissioning on the injector diagnostic plate, a good agreement with the TRACEWIN simulations was observed [12]. BEM measurements were compared to TRACEWIN simulations at rebuncher voltage ranging from 15 to 115 kV (nominal value about 35 kV) [21]. The agreement of the measurement was confirmed with a maximum error of ±3% when the beam is bunched. These results were validated with the proton beam in 2019.

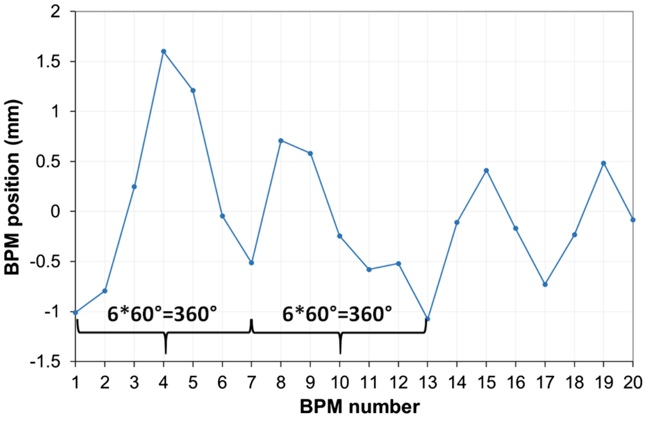

FIG. 7. Vertical beam position along the SC linac for the 16 kW beam.

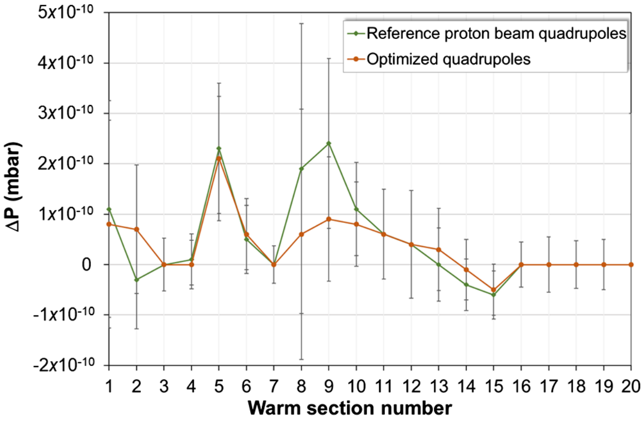

FIG. 8. Pressure variation in the warm sections of the SC linac with the MEBT quadrupoles for the reference proton beam (green) and after optimization (orange).

Figure 9(a) shows the reference longitudinal acceptance of the SPIRAL2 SC linac (green dots). It can be seen that the acceptance boundary on the left is lower than that on the right. Figure 9(b) shows the beam loss measurement on the BLMs located in the HEBT line at high energy as a function of a phase shift in rebuncher #3. The acceptance asymmetry observed in the simulation is clearly confirmed by the measurements, and it is increased by the fact that a shift of the rf phase of the rebuncher also introduces a small variation in the beam energy at the SC linac entrance.

The longitudinal matching improvement was achieved experimentally by changing the voltage of rebuncher #3. The BLM counts were observed as it varied. It has been noted that for a few BLMs the counts decreased as the rebuncher voltage was increased from 29.6 (reference value) to 35.6 kV. Taking this into account, the BLM measurements and the pressure variations were studied, the results are presented in Fig. 10. First, the decrease in BLM counts can be seen between low and high β sections (red circle in Fig. 10), where the envelope margin is the lowest, at the end of the SC linac (blue circle), and in the HEBT line (purple circle). This matching allowed to reduce longitudinal emittance growth and then lower losses at high energy (blue circle). Simulations show that particles out of the bucket in between the two sections result in losses in the HEBT line, this is confirmed by the BLMs measurements (purple circle). In parallel, the pressure variation showed a decrease in losses in two SC linac

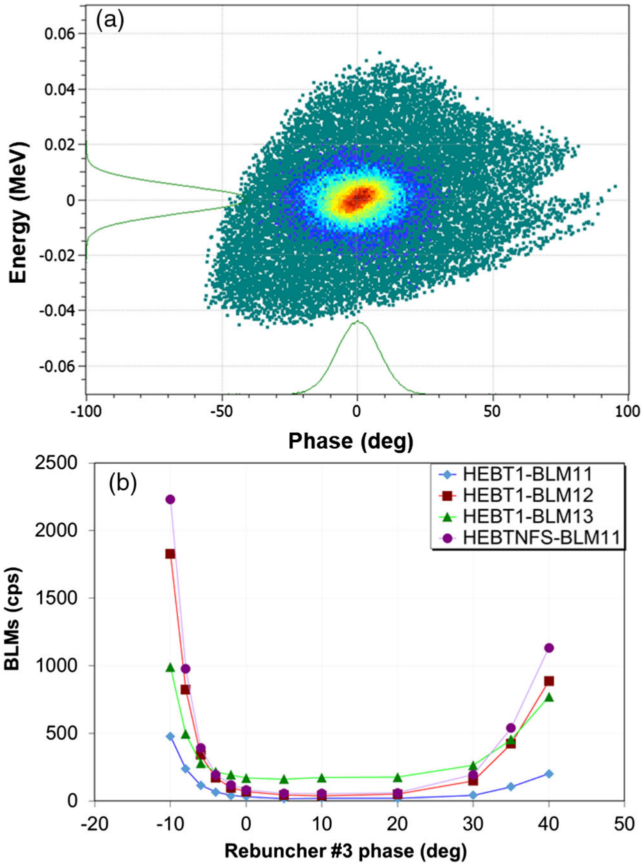

FIG. 9. (a) Longitudinal acceptance of the SC linac and (b) measurement of the losses for the HEBT line as a function of rebuncher #3 phase.

low β sections, around cryomodules #4 and #7, as shown in Fig. 11.

V. LLRF SETTINGS

The beam loading generated by beam currents tends to decrease the accelerating fields and detune the cavities, with significant final energy reduction and beam loss rise. Figure 12(a) shows the exponential loss rise as soon as few mA intensities are reached when insufficient feedback is applied.

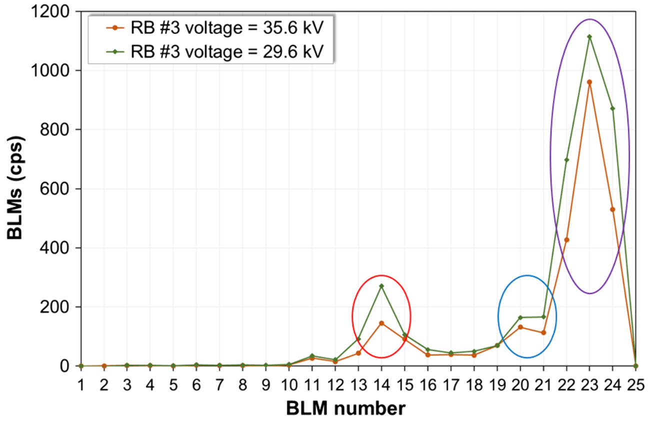

FIG. 10. BLMs count rate as a function of the voltage of rebuncher #3, 35.6 kV (orange) and 29.6 kV (green).

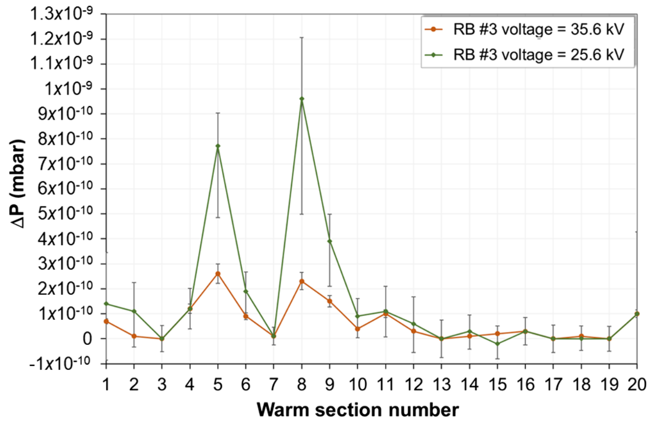

FIG. 11. Pressure variation in the SC linac warm sections as a function of the rebuncher #3 voltage, 35.6 kV (orange) and 29.6 kV (green).

According to the reference simulations, 1% stability of the cavity fields was required but a sufficiently high feedback gain could not be achieved due to noises

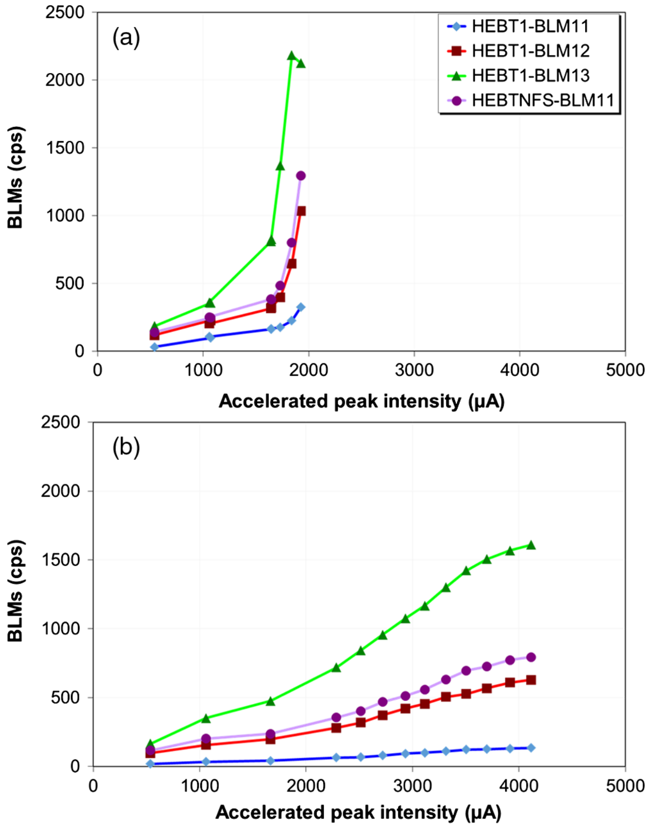

FIG. 12. Losses in the HEBT lines a function of the beam peak intensity: (a) with insufficient gain feedback for the cavity fields and (b) for an optimized LLRF control.

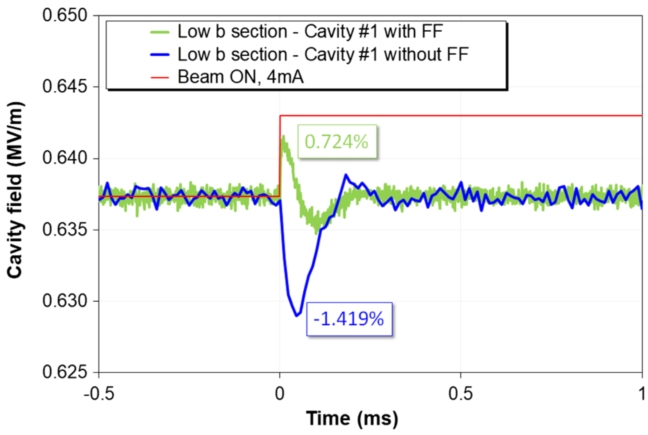

FIG. 13. Residual perturbation on the accelerating field of cavity #1 in the low β section with a 4.1 mA proton beam with and without feedforward (FF).

generating cavity tuning system instability. At maximum feedback gain, the residual field error was still about −2.4%. Feedforward (FF) was then added to the first cavities, which are more affected by beam loading as they work at a low field.

Figure 13 shows the residual perturbation on the accelerating field for the first low β cavity. The green line shows the effect of adding the FeedForward (FF). Cases with FF are easy to identify as the first spike is positive. The FF algorithm that is used stores I and Q components of the modulator signals at the end of the previous pulse and applies them at the beginning of the next pulse to match the required higher power and different phase. A beam presence signal provides the rising and falling edges of the beam pulses. As shown in Fig. 13, FF divided by two the residual perturbation that is now ~0.7% at 4 mA and would be just below 1% at 5 mA for the first cavities. Room for improvement still exists, mostly from a better adjustment of the synchronization delay between the beam presence and the feedback signal.

The LLRF algorithm also stores the mistuning induced by the beam loading and corrects it using the cold tuning system at each pulse to minimize the required rf power.

Figure 12(b) shows the benefits when all the LLRF feedback and feedforward are correctly set. This figure shows that losses in the HEBT are now kept at a very low level. The linearity of the curve with an increasing pulse length confirms that there is no source of additional losses to be considered. It should be also noted that the linear increase in BLM count rate in the HEBT line is mainly due to neutrons backscattered from SAFARI. The minor variations of the linearity can be explained as follows: As the SC linac is set for 5 mA, above 3.5 mA, the emittance effect is compensated by the better matching of the SC linac, with the intensity and provide an improvement in the trend of the losses. This is attributed to the fact that the associated emittance generates more transverse losses.

VI. BEAM POWER RAMP-UP

Several parameters were recorded during the beam power increase to study (i) linac beam transmission, (ii) beam position and ellipticity, (iii) losses in the SC linac and in the HEBT line, and (iv) beam dump temperatures.

A. SC linac transmission

The beam transmission is measured by two ACCT located at the entrance and exit of the SC linac. The electronics is optimized with a direct comparison of the two ACCT signals to provide better precision.

Figure 14 shows the temporal evolution of the transmission in the SC linac with an average value above 100% with a measurement accuracy of 3 μA, demonstrating the precision limits. It can be seen that the average intensity and noise level evolve in correlation with an increasing pulse length. This is due to the calibration measurement made without a beam between pulses (clamps) and evolves as the pulse length increases. The noise increase observed at 15:35 is due to a decrease in the number of clamps as the beam time increases.

B. Beam positions

Figure 15 shows the beam positions in the vertical plane during the 2, 10, and 16 kW beam power periods. With a maximum value of 2 and 1 mm in the vertical and horizontal planes, respectively, the beam was considered as sufficiently stay aligned to well below the authorized losses. The differences between the measurements are mainly due to the quadrupole retuning in the MEBT line after the power increase to 10 kW and beam alignment.

C. BLMs

Figure 16(a) shows loss measurements by each BLM at 2, 10, and 16 kW, after subtraction of the x-ray background from the cavities. It can be seen that higher losses in the SC

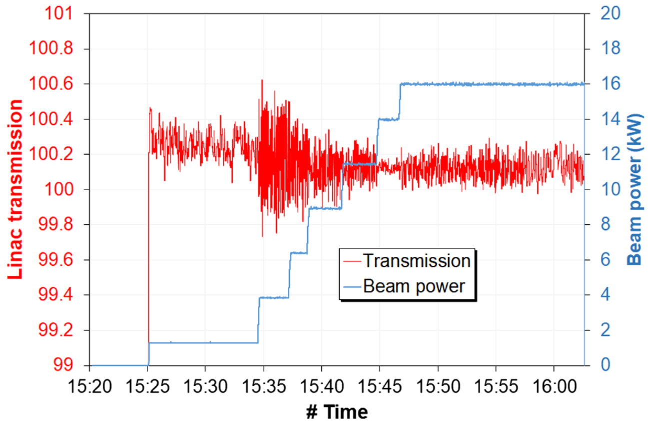

FIG. 14. Transmission in the SC linac (red) and beam power (blue) during the beam power ramp-up to 16 kW.

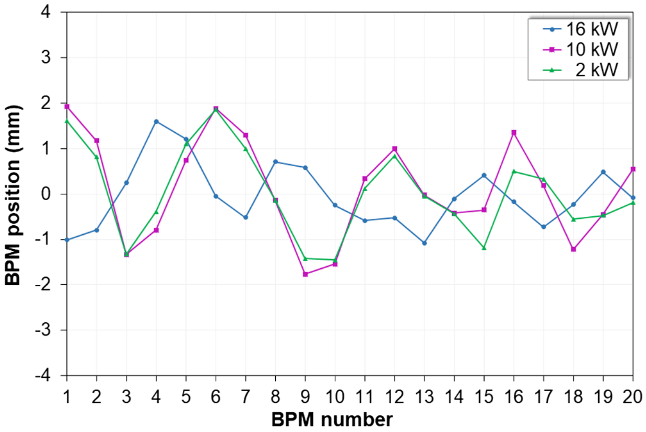

FIG. 15. Beam position in the vertical plane along the SC linac for 16 kW (blue), 10 kW (violet), and 2 kW (green).

linac occur between low and high β sections and in the last part of the high β section. This is in agreement with the acceptance decrease in the transition zone shown in Fig. 16(b).

Furthermore, these measurements confirm the results obtained in a statistical study performed for SPIRAL2. This study was carried out for a $^2H^+$ beam at nominal current (5 mA) with 2.5×10^9 particles, showing that the low level losses in the linac occur in the transition zone between the low and high β sections as presented in Fig. 17. The particles are stripped out of the bucket in the first section of the linac. In order to have a full understanding of the losses, the study was performed with errors in the cavities (1%, 1° phase). It was found that the cavity tuning error is responsible for 20% of the losses, while the longitudinal distribution at the RFQ exit is responsible for about 80% of the losses. Figure 18 demonstrates this origin, as shown in the distribution of the losses in the linac brought back to the exit of the RFQ, and demonstrates the main origin of the linac losses.

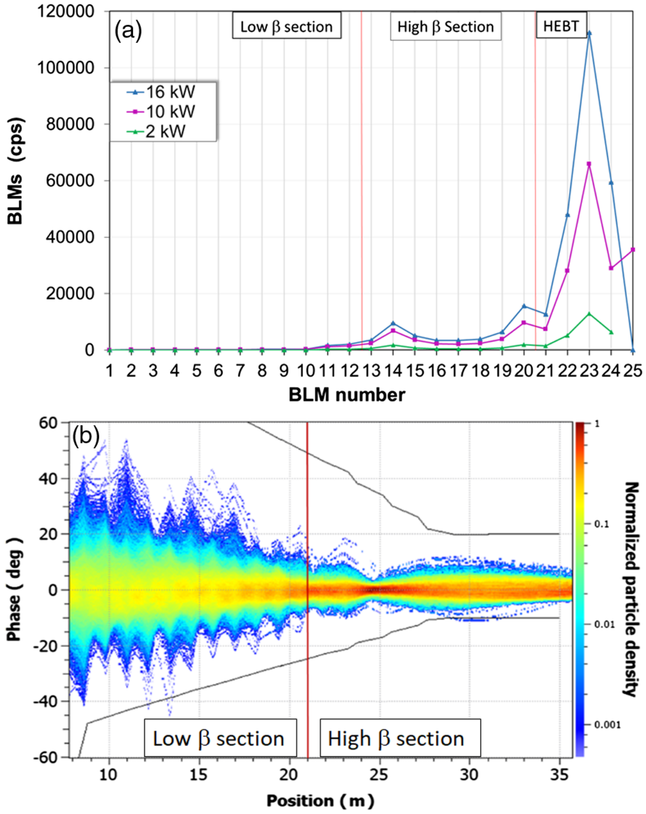

FIG. 16. (a) Count rate for each BLM at 16 kW (blue), 10 kW (violet), and 2 kW (green) beam power and (b) beam density in the longitudinal plane of a proton beam. Dark lines are the ϕ_s and $-2\phi_s$ limits.

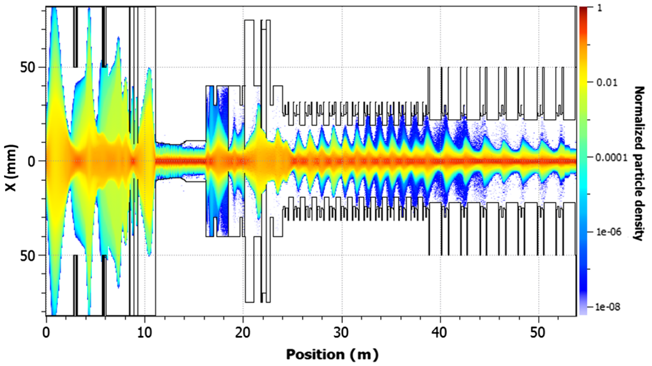

FIG. 17. Horizontal particle density of a 5 mA $^2H^+$ beam for the reference simulation with 2.5×10^9 particles.

The BLM count in the HEBT section comes from a different explanation, as it is mainly due to the neutrons coming back from SAFARI, as explained before.

The counts per second from the power increase to 16 kW were extrapolated to 100% duty cycle. Figure 19 shows the

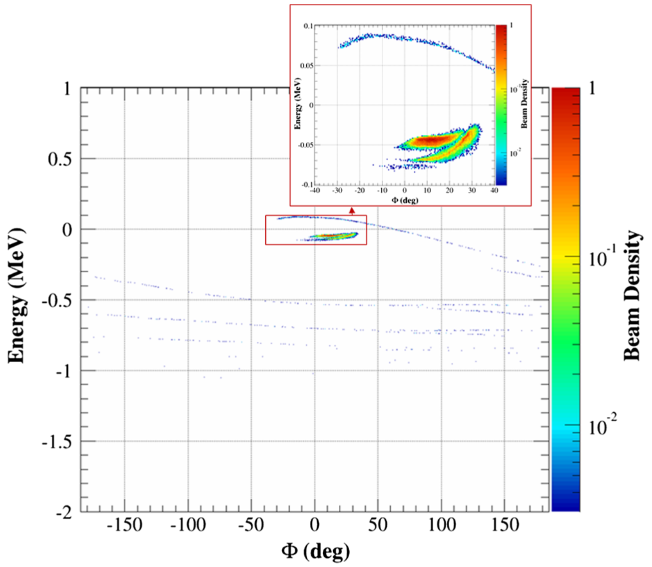

FIG. 18. Distribution of the losses in the linac brought back to the exit of the RFQ.

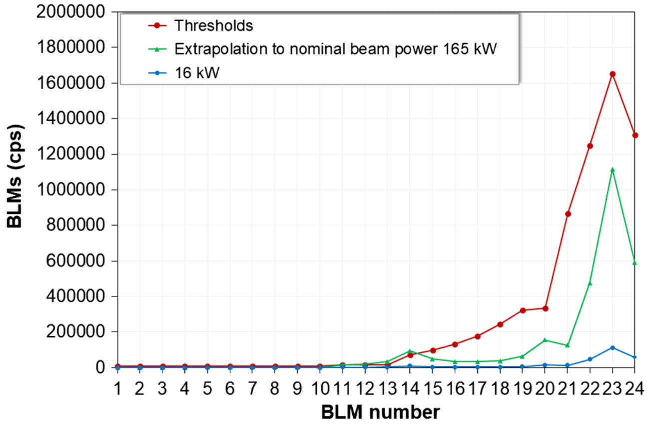

FIG. 19. BLMs count rate for the proton beam at 16 kW (blue), extrapolation to 100% duty cycle (green), and BLMs thresholds (red).

beam loss measurements at 16 kW, the linear extrapolation to 100% duty cycle, and the thresholds at 1 W/m for linac operation. The comfortable margin versus this 1 W/m limit indicates that the beam power ramp-up to 16 kW demonstrates the feasibility to work with the nominal 165 kW (cw) proton beam.

D. Pressure variations in the SC linac

Figure 20 shows the pressure variations along the SC linac. There are two peaks observable during the 10 kW period, one in warm section #5 in the middle of the low β section and another in warm section #8, at the end of this section.

The pressure variation is a sensitive diagnostic that reacts in less than a second and is very useful to minimize beam losses [22]. Further studies are ongoing in order to calibrate the pressure variation in terms of beam losses in W at various beam energies. For that purpose, a 1 W $^2H^+$ beam was lost in various warm sections at different beam energies. The analyses are ongoing and the results will be published soon. The MEBT-SC linac matching improvements done after the 10 kW tuning, much more than the alignment, explains significant loss reductions in the low β section.

These results confirm that the measurement of pressure variations is a very good tool for the low β section of the SC linac, where BLMs are not sensitive.

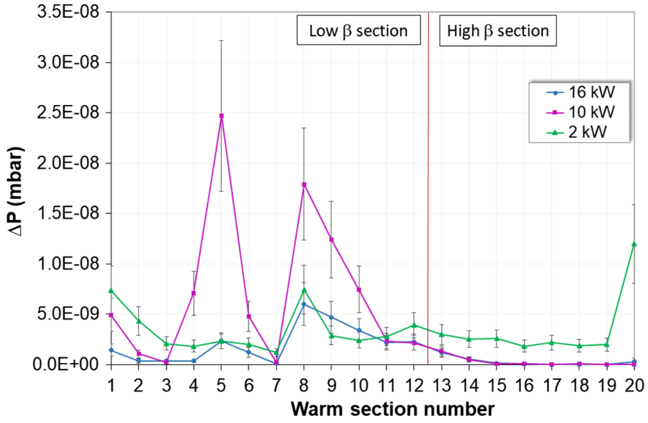

FIG. 20. Pressure variations at 16 kW (blue), 10 kW (violet), and 2 kW (green).

E. SAFARI beam dump

SAFARI is the main beam stop at the end of the SC linac. It is designed for a uniform distribution of 200 kW beam power [4] and is equipped with K01 thermocouples, whose working range goes up to 350 °C. However, according to the thermal studies carried out [23], taking into account the material conditions, the maximum operating parameters should be a copper temperature of 141 °C, permissible stress of 180 MPa, and a water temperature of 120 °C. The temperature with and without beam was recorded for each beam power period to control the temperature rise. In order to obtain more detailed information from the data, the position of each thermocouple along the beam dump from the input (large size) to the end (small size) is represented as shown in Fig. 21. The higher temperature in the lower right zone shows that the beam was not perfectly aligned during the 16 kW run. The elevated temperature at the target entrance was probably due to a larger than expected beam vertical size.

The time slot for the power ramp-up was very short and the beam distribution was not optimized due to the high power margin. To reach the nominal power, these issues should be addressed more carefully to keep the maximum temperature below 141 °C in all thermocouples.

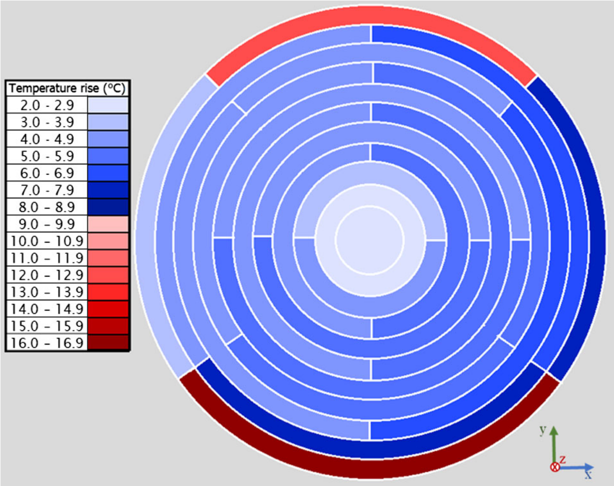

FIG. 21. Beam view of SAFARI. The colors represent the temperature rise in each thermocouple at 16 kW, light blue colors lower temperatures and red colors higher temperatures.

VII. SUMMARY

The SPIRAL2 SC linac has been successfully commissioned with a 16 kW proton beam representing 10% of the maximum beam power. This 16 kW beam power was achieved with long pulses (12.6 ms/100 ms), representative of a cw operation. The proton beam was accelerated to 31.90 ± 0.05 MeV with 100% ($\pm 3\ \mu$A) transmission. The maximum beam power was limited to stay below the authorized activation of the SAFARI beam dump. The losses were progressively reduced well below the threshold which demonstrates the feasibility to work at a nominal beam power (165 kW, cw). At each commissioning step, the measured beam parameters have been in good agreement with the reference simulations.

One must conclude that the SPIRAL2 commissioning success is due to a large collaboration in which each member has provided a stone without which it would not be possible. To make it short, one can also say that a detailed analysis of the transverse and longitudinal tunings and the improvement of the LLRF feedback and feedforward systems have been two important technical steps for this success.

ACKNOWLEDGMENTS

The authors would like to thank all the GANIL staff and external collaborators for the huge amount of work that led to a successful SPIRAL2 SC linac commissioning. Particular thanks to the GANIL Operator Team members for their key role on this completely new and different machine.

[1] H. Goutte and N. Alahari, Microscopes for the Physics at the Femtoscale: GANIL-SPIRAL2, Nucl. Phys. News **31**, 5 (2021).

[2] P. Dolégiéviez *et al.*, Spiralling into the Femtoscale, CERN Courier **60**, 39 (2020), https://cerncourier.com/wp-content/uploads/2020/11/CERNCourier2020NovDec-digitaledition.pdf.

[3] J.-M. Lagniel, Advances of the Spiral 2 Project, in *Proceedings of the 13th International Conference on Heavy Ion Accelerator Technology, Yokohama, Japan, 2015* (JACoW Publishing, Geneva, Switzerland, 2016), pp. 148–152, https://accelconf.web.cern.ch/AccelConf/HIAT2015/papers/tua2i01.pdf.

[4] E. Schibler and L. Perrot, SAFARI, an optimized beam stop device for high intensity beams at the Spiral2 Facility, in *Proceedings of the 2nd International Particle Accelerator Conference, San Sebastián, Spain, 2011* (JACoW Publishing, Geneva, Switzerland, 2011), pp. 1162–1164, https://accelconf.web.cern.ch/IPAC2011/papers/tupc070.pdf.

[5] X. Ledoux *et al.*, The neutrons for science facility at SPIRAL-2, EPJ Web Conf. **146**, 03003 (2017).

[6] A. Drouart *et al.*, The Super Separator Spectrometer (S3) for SPIRAL2 stable beams, Nucl. Phys. **A834**, 747 (2010).

[7] A. Drouart *et al.*, Fusion-evaporation studies with the Super Separator Spectrometer (S3) at Spiral2, EPJ Web Conf. **17**, 14004 (2011).

[8] P.-E Bernaudin *et al.*, Status of the SPIRAL 2 Superconducting LINAC, in *Proceedings of the 1st International Particle Accelerator Conference, Kyoto, Japan, 2010* (JACoW Publishing, Geneva, Switzerland, 2010), https://accelconf.web.cern.ch/IPAC10/papers/mopd025.pdf.

[9] R. Ferdinand *et al.*, The SPIRAL 2 Superconducting Linac, in *Proceedings of the 24th Linear Accelerator Conference, LINAC-2008, Victoria, Canada, 2008* (JACoW Publishing, Geneva, Switzerland, 2008), pp. 196–198, https://jacow.org/LINAC08/papers/MOP053.pdf.

[10] G. Olry *et al.*, Spiral2 cryomodules B tests results, in *Proceedings of the 16th International Conference on RF Superconductivity, SRF2013, Paris, France, 2013* (JACoW Publishing, Geneva, Switzerland), pp. 95–99, https://hal.archives-ouvertes.fr/in2p3-00867506.

[11] C. Marchand, Performances of Spiral2 low and high beta cryomodules, in *Proceedings of the 17th International Conference on RF Superconductivity* (JACoW Publishing, Geneva, Switzerland, 2015), pp. 967–972, https://accelconf.web.cern.ch/AccelConf/SRF2015/papers/weba04.pdf.

[12] R. Ferdinand *et al.*, Final results of the SPIRAL2 injector commissioning, in *Proceedings of the 10th International Particle Accelerator Conference, IPAC-2019, Melbourne, Australia, 2019* (JACoW Publishing, Geneva, Switzerland, 2019) pp. 848–851, http://accelconf.web.cern.ch/ipac2019/papers/MOPTS006.pdf.

[13] M. Di Giacomo, R. Ferdinand, B. Jacquot, J.-M. Lagniel, X. Ledoux, O. Kamalou, G. Normand, and A. Orduz, Proton beam commissioning of the SPIRAL2 single bunch selector, J. Instrum. **15**, T12011 (2020).

[14] A. K. Orduz *et al.*, Beam commissioning SPIRAL2, in *Proceedings of the 12th International Particle Accelerator Conference, IPAC-2021, Campinas, SP, Brazil* (JACoW Publishing, Geneva, Switzerland, 2021), pp. 2540–2543, https://jacow.org/ipac2021/papers/WEXB05.pdf.

[15] S. Leloir *et al.*, Measurement uncertainty assessments of the SPIRAL2 ACCT/DCCT, in *Proceedings of IBIC2016* (JACoW Publishing, Barcelona, Spain, 2016), pp. 712–714, https://www.jacow.org/ibic2016/papers/wepg39.pdf.

[16] C. Jamet *et al.*, SPIRAL2 diagnostic qualifications with RFQ beams, in *Proceedings of the 8th International Beam Instrumentation Conference, IBIC-2019, Malmö, Sweden, 2019* (JACoW Publishing, Geneva, Switzerland), pp. 188–192, http://jacow.org/ibic2019/papers/mopp036.pdf.

[17] C. J. Werner, J. S. Bull, and C. J. Solomon, Monte Carlo N-Particle Transport, MCNP6.2 Release Notes LA-UR-18-20808, Los Alamos National Laboratory (2018), https://www.osti.gov/servlets/purl/1419730.

[18] E. Mahner, Review of heavy-ion induced desorption studies for particle accelerators, Phys. Rev. ST Accel. Beams **11**, 104801 (2008).

[19] S. Bilgen, Dynamic pressure in particle accelerators: Experimental measurements and simulation for the LHC, Ph.D. thesis, Université Paris-Saclay, 2020, https://tel.archives-ouvertes.fr/tel-03362698/file/93615_BILGEN_2020_archivage.pdf.

[20] D. Uriot and N. Pichoff, TRACEWIN, Le Commissariat à l'énergie atomique et aux énergies alternatives (CEA), https://dacm-logiciels.fr/ (2015).

[21] G. Normand *et al.*, SPIRAL2 RFQ bunch lengths and longitudinal emittance measurements, in *Proceedings of the 10th International Particle Accelerator Conference, IPAC-2019, Melbourne, Australia, 2019* (JACoW Publishing, Geneva, Switzerland, 2019), pp. 1944–1947, http://accelconf.web.cern.ch/ipac2019/papers/TUPTS007.pdf.

[22] H. Kollmus *et al.*, Energy scaling of the ion-induced desorption yield for perpendicular collisions of Ar and U with stainless steel in the energy range of 5 and 100 MeV/u, J. Vac. Sci. Technol. A **27**, 245 (2009).

[23] E. Schibler *et al.*, Design of a high energy beam stop for spiral2, in *Proceedings of the 25th Linear Accelerator Conference, LINAC 2010, Tsukuba, Japan* (KEK, Tsukuba, Japan, 2010), https://accelconf.web.cern.ch/LINAC2010/papers/mop097.pdf.